TRIFIC: The TRIUMF Fast Ion Counter

A. Chester[a,1,*], J. Smallcombe[a,b], J. Henderson[a,2], J. Berean-Dutcher[a],
N. Bernier[a,c], S. S. Bhattacharjee[a], A. B. Garnsworthy[a], S. Georges[a],
S. A. Gillespie[a], G. Hackman[a], B. Olaizola[a], O. Paetkau[a], C. J. Pearson[a],
B. Undseth[a], D. Yates[a,c]

[a]*TRIUMF, 4004 Wesbrook Mall, Vancouver, British Columbia, Canada, V6T 2A3*
[b]*Oliver Lodge Laboratory, University of Liverpool, Liverpool L69 9ZE, United Kingdom*
[c]*Department of Physics and Astronomy, University of British Columbia, Vancouver, B.C., Canada, V6T 1Z1*

Abstract

The TRIUMF Fast Ion Counter (TRIFIC) is a tilted-grid gas counter detector for identifying the impurities in radioactive ion beams (RIBs). Placed at zero degrees downstream of a primary reaction target at the TRIUMF ISAC-II facility, TRIFIC provides accurate Z identification of beam species on an event-by-event basis at a rate of up to 5×10^5 particles per second and functions as a beam composition monitor at rates up to 5×10^7 particles per second. With this additional level of diagnostics, RIB experiments at TRIUMF are able to reach levels of sensitivity not previously possible. Details regarding the construction and instrumentation of TRIFIC as well as results from the commissioning of the detector are presented.

Keywords: Gas Detector, Ionization chamber, Radioactive ion beams, Particle identification

*Corresponding Author: chester@frib.msu.edu
[1]Present Address: National Superconducting Cyclotron Laboratory, Michigan State University, East Lansing, Michigan 48824, USA
[2]Present Address: Lawrence Livermore National Laboratory, Livermore, CA 94550, USA

1. Introduction

Radioactive ion beam (RIB) facilities have created many opportunities to study nuclei far from stability, critical to advancing the understanding of nucleosynthesis, nuclear structure, and reactions. RIB production at TRIUMF, Canada's particle accelerator centre, is achieved through the isotope separation on-line (ISOL) technique: a driver beam–in this case protons from the TRIUMF 520 MeV H^- cyclotron–impinges on a heavy target material. Isotopes created by reactions in the target are extracted and ionized, separated by mass-to-charge ratio, and delivered to an experimental station. Along with the isotope of interest, isobars and isotopes with a similar mass-to-charge ratio may all reach an experiment. Some beams delivered to the ISAC-II facility at TRIUMF require charge state breeding, which can introduce additional stable beam contaminants. As such, it is essential to distinguish the RIB isotope of interest from any contaminant species which may also be present in the beam. Many experiments which take advantage of RIBs are run in so-called inverse kinematics, where a heavy beam nucleus undergoes a reaction on a light target, resulting in forward-focused reaction products. In such applications beam identification can be achieved by placing a detector at zero degrees with respect to the beam axis.

Gas ionization chambers are ideal for this purpose due to their sensitivity to the characteristic range and energy loss of ions, radiation hardness, and the relatively fast signal risetimes which allow for the operation of specially-constructed detectors at high beam intensity. Following the development of several successful fast ion counters [1–4], the TRIUMF Fast Ion Counter (TRIFIC) was designed and constructed to couple with experiments using the TIGRESS γ-detector array [5] at TRIUMF's ISAC-II facility [6].

TRIFIC is a compact cylindrical gas counter, mounted along the beam axis directly downstream of TIGRESS and used to identify beam-like ion species based on their characteristic energy loss profile. Signals from the detector are read out through custom-built low-noise preamplifiers and further analyzed using a GRIFFIN-style digital data acquisition system [7]. These aspects of the detector, which distinguish it from other recently developed detectors presented in Refs. [1–4], are discussed further in Secs. 2 and 3. TRIFIC is designed for operation in two modes. In the "recoil tagging" operational mode, beam-like reaction products are identified on an event-by-event basis in coincidence with signals from TIGRESS and ancillary charged-particle detection systems such as the SHARC [8] and Bambino [9] segmented silicon detector arrays. At high incident beam rates, TRIFIC may be operated in the so-called "beam monitor" mode, where the intense beam is attenuated (see Sec. 2) and contaminant beam species may be quantified in real time. These two modes of operation are discussed in the subsequent sections in the context of typical types of experiments performed at TIGRESS.

1.1. Transfer reaction experiments with TRIFIC

Reactions in which one or two nucleons are added to or removed from a nucleus (so-called "direct" reactions such as (d,p) or (t,p)) provide a powerful tool for studying the single particle structure of exotic nuclei at RIB facilities such as TRIUMF (see, e.g. Ref. [10]). Typically performed at 5–10 MeV/A, the direct reaction of interest will often be contaminated by other channels, such as compound reactions or other direct reaction channels, even with a contaminant-free primary beam. Due to the reaction kinemat-

3

ics, recoiling nuclei produced in the reactions are forward focused and can be observed by placing a detector at zero degrees relative to the beam axis. Operating TRIFIC in "recoil tagging" mode allows for the separation of the reaction products of interest from background reactions following un-ambiguous identification of the desired transfer reaction products in the TRIFIC detector. Coincident detection of the reaction products using mul-tiple detection systems (e.g. TIGRESS, TRIFIC, and SHARC) provides a clean tag of the reaction.

Additionally, the use of TRIFIC as a zero-degree "recoil tagging" detec-tor has a significant advantage over fast scintillator detectors which have been previously employed for this purpose (see Ref. [11]) because cycling gas through TRIFIC ensures that the detector performance is stable over long periods of time. This is in contrast to the significant loss in performance and efficiency of scintillator detectors as they become radiation damaged from exposure to reaction products and un-reacted beam. TRIFIC in the "recoil tagging" mode is designed to operate with beam intensities up to 1 Mpps with a resolving power of $Z/\Delta Z \geq 40$.

1.2. Coulomb excitation experiments with TRIFIC

Great progress is being made in understanding the structure of nuclei far from stability by studying Coulomb excitation (Coulex), where nuclear electromagnetic matrix elements are determined directly from sub-barrier collisions [12–15]. An important question of normalization arises during the analysis of such experiments. It is common to normalize to known strengths of transitions in the target nuclei which are excited simultaneously with the beam in the Coulex process [13]. However to perform such a normalization

4

it is important to have an accurate measurement of both the make-up of the target and of the beam. Moreover, the composition of the beam can change during the measurement period. The precision to which one knows the beam composition is often a significant source of systematic uncertainty, which can constitute a serious limitation to the accuracy of the final measurement.

With this in mind, TRIFIC can be used to get an accurate synchronous (real-time) measurement of the beam constituents on a run-by-run basis throughout the course of an experiment. This has the advantage over sporadic asynchronous measurement (i.e. snapshots of the beam composition), in that rapid shifts in the beam composition which are common due to the complex chemical nature of ISOL targets at facilities such as TRIUMF-ISAC, can be correctly accounted for in order to give the most accurate integrated yields over time. When in this "beam monitor" mode of operation TRIFIC requires only a representative sample of the full beam rate. Furthermore, in such experiments the selection of particles being detected is dominated by un-reacted beam particles which suffer significantly less angular dispersion than that of reaction products. As such, the tilt of the grids (see Sec. 2) has a smaller effect on the range measurement of the particles and an overall higher $Z/\Delta Z$ resolving power is achieved. One final boon of this operational mode is that different species need not be clearly resolved on an event-by-event basis, as only a ratio measurement is required. This enables the device to be operated closer to the resolving limit.

2. Detector construction

TRIFIC is a tilted-grid gas ionization chamber, consisting of multiple wire grids mounted in a 73 mm radius cylindrical chamber, typically oper-
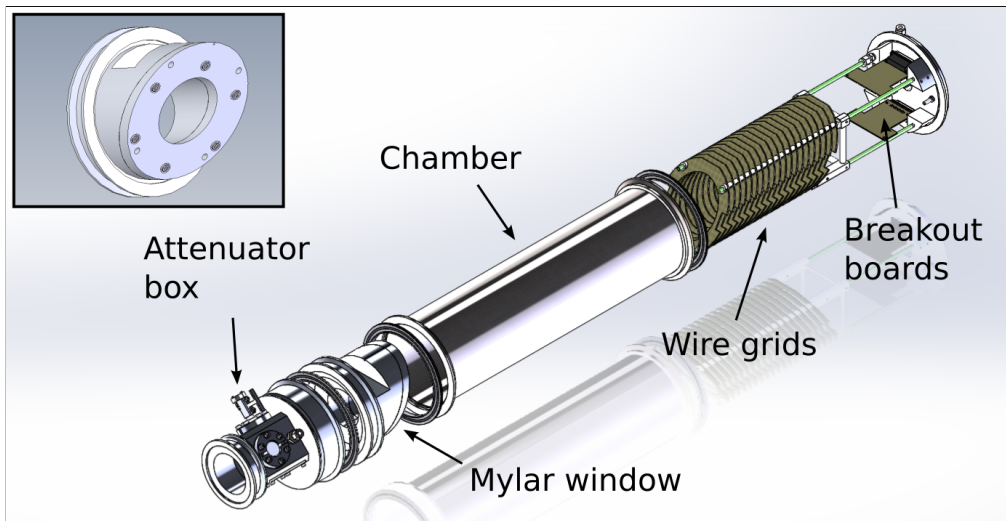
Figure 1: Exploded view of the TRIFIC detector with key components labelled. A description of the components is given in the text. The inset shows the downstream side of the Mylar entrance window. Beam enters the detector from the lower left. (Color online).

ated using 50–100 Torr of CF_4 gas. TRIFIC was developed from the design of a similar detector used at the HRIBF facility at Oak Ridge National Laboratory [1]. An upstream attenuator box houses two ×0.1 attenuator foils which can be used together to accommodate beam intensities up to 50 Mpps in the "beam monitor" operational mode along with a Faraday cup for beam tuning and diagnostics. A schematic drawing of the detector's important constituent parts is shown in Fig. 1. A cross-sectional diagram is shown in Fig. 2, and a photo of the detector components presented in Fig. 3.

The TRIFIC electrode grids are constructed from 2.6 mm thick PCB boards with an elliptical opening tilted by 30° such that the electrodes present a circular profile with a 50 mm radius along the beam axis. Tilting
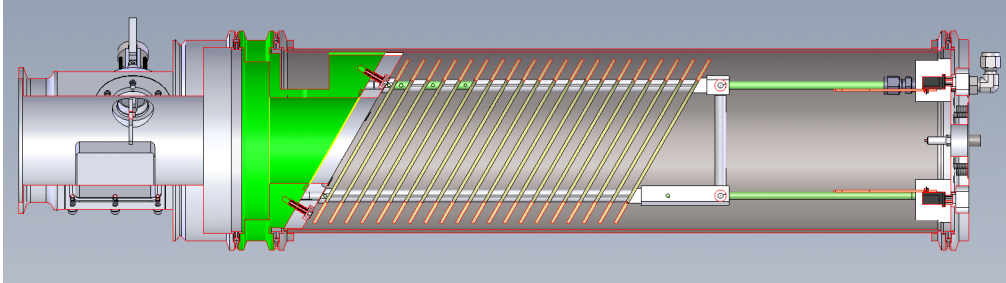
6

Figure 2: A cross-section of the TRIFIC detector showing the various components described in Sec. 2. The Mylar entrance window mount is highlighted in green. Beam enters from the left. (Color online).

the electrodes aligns the electric field such that electrons and ions created within the gas drift away from the beam axis thereby minimizing recombination effects. Fifty 20 μm diameter gold-coated tungsten wires are soldered to the electrodes at a 2 mm pitch giving a total transmission per grid of 99%. TRIFIC is nominally operated with 24 electrodes, which are individual mounted on G-10 rods and separated by 10 mm PEEK spacers [3]. The 24 grid setup can accommodate ion ranges up to 30 cm with a total transmission of ≈79% from the first to the last grid allowing for good flexibility in detecting ions in the 5–10 MeV/A range achievable at TIGRESS. For example, ^{20}Ne at 5.25 MeV/A (105 MeV), ^{40}Ar at 5.75 MeV/A (230 MeV), and ^{84}Kr at 6.31 MeV/A (530 MeV) all have a range of 30 cm in 95 Torr of CF_4 gas [16].

To create the electric field of TRIFIC different bias is applied to alternating grids, creating 2 groups of electrodes (cathodes and anodes). The capacitance between adjacent grids was measured to be 15.8(5) pF. High

---

[3]Up to 48 grids can be accommodated using 5 mm PEEK spacers that are also available but were not used in the presented work.
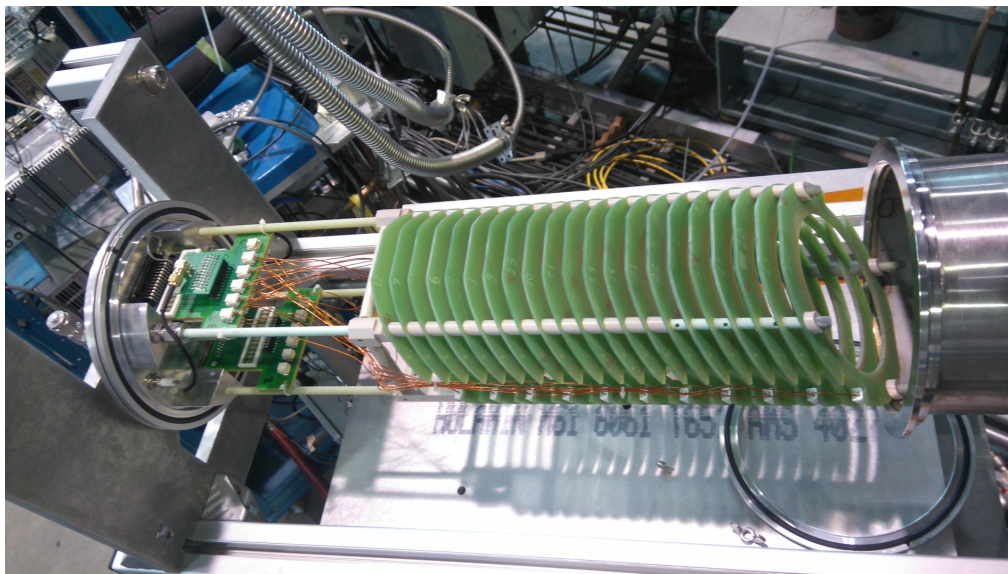
7

Figure 3: A photo of the interior components of the TRIFIC detector labelled in Fig. 1. The grids are described in detail in Sec. 2. The breakout boards containing the internal RC buffer circuits are visible on the left of the figure. The beam enters the detector from the right in this photograph. (Color online).

voltage bias is applied separately to the cathode and anode grids via two RG-59 cables with SHV connectors which are connected to a mesytec MHV-4 power supply [17]. External high-pass filters consisting of a 1 MΩ resistor (R_{HV}) and 1 μF capacitor (C_{HV}) are used to suppress low-frequency noise from the power supply. Signals from individual electrodes are read out through an internal RC buffer circuit composed of an exchangeable 1 MΩ resistor (R_B), through which HV bias is delivered, and a 47 pF capacitor (C_B), which isolates the HV from the signal output. These components are highlighted on the block diagram of the detector electronics shown in Fig. 4. The buffer capacitors are vacuum potted with epoxy for isolation and to prevent arcing at low operating pressure. The buffer circuit can accommodate up to 4 groups of 12 signals giving a maximum readout capacity of 48 individual channels.

TRIFIC is separated from the beamline vacuum by an entrance window with a radius of 35 mm which protrudes inside the chamber and is tilted at 30° similar to that described in Ref. [1]. A schematic of the window is shown on the inset of Fig. 1. The window opening is located 2 cm upstream from the first set of electrode wires and consists of aluminized Mylar which is fixed in place with a bracket machined to match the 30° tilt and is sealed using an O-ring. Windows experience some limited distortion towards the target while under pressure. Six μm thick Mylar windows were tested at pressure differentials up to 300 Torr.

2.1. Biasing scheme

The effect of different biasing schemes on the electron transport in TRIFIC was investigated using the Garfield++ simulation package [18].
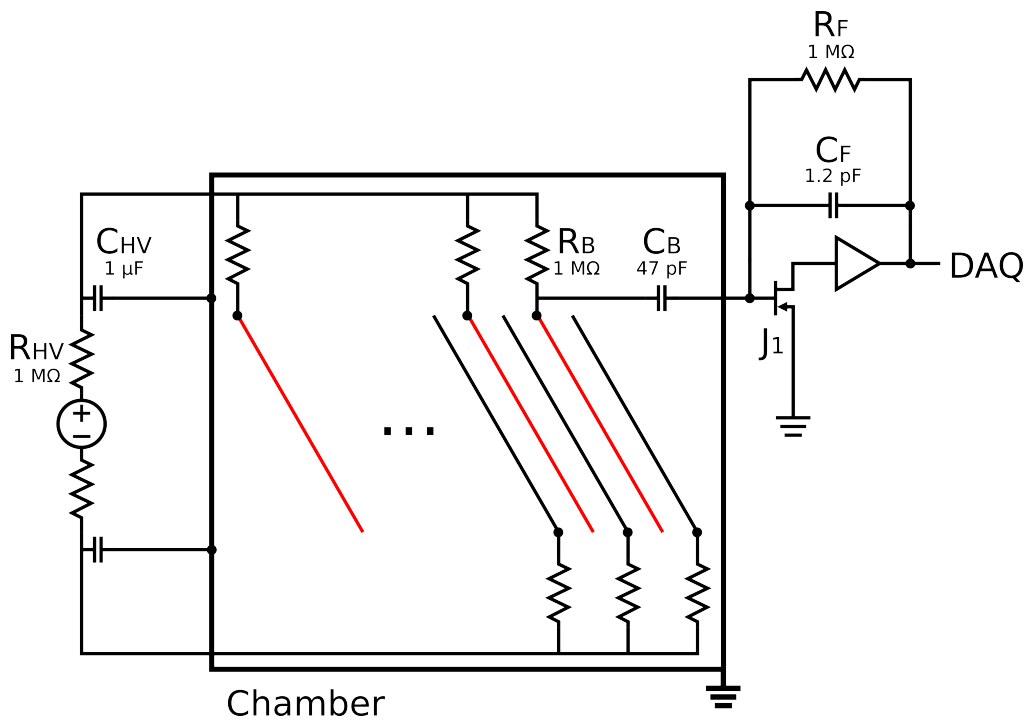
9

Figure 4: Block diagram of TRIFIC showing the HV filter (R_{HV} and C_{HV}) and buffer circuit (R_B and C_B) described in Sec. 2 as well as a single channel of the preamplifier circuit (J_1, R_F and C_F) described in Sec. 2.2. Some typical component values are shown. For details on the specific sub-systems, refer to the text. The cathode and anode grids are shown in black and red, respectively. (Color online).

Field maps and electron drift lines calculated by Garfield++ for a constant potential difference of 244 V between the electrode grids are shown in Fig.5. During the commissioning tests, it was demonstrated that a negative bias voltage on the first electrode grid (initially at ground) significantly improved the signals recorded on the second. This improvement arises due to the suppression of slow charge collection on the second grid from electron-ion pairs created in the region between the Mylar window and the first electrode. As expected, the Garfield++ simulations confirmed that supplying a negative bias to the first electrode group creates an electric field which repels electrons created from ionization upstream of the first grid. Calculated drift lines demonstrating this effect are shown in the bottom two panels of Fig. 5.

The optimal biasing scheme determined from the simulations was to split the bias evenly across the anodes and cathodes. This scheme minimizes the potential difference between the anodes/cathodes and the detector elements which are kept at ground, such as the chamber and window. As a result, sparking between these elements is minimized and stable running conditions with higher electric fields in the active volume of the detector can be achieved. Additionally, the fringe effects at the edges of the grids are also minimized as shown in Fig. 5.

2.2. TRIFIC electronics

A set of 24-channel, low-noise, two-stage gain charge-sensitive preamplifier modules, instrumented with a JFET for noise reduction, have been designed and constructed by the TRIUMF Electronics Development Group for
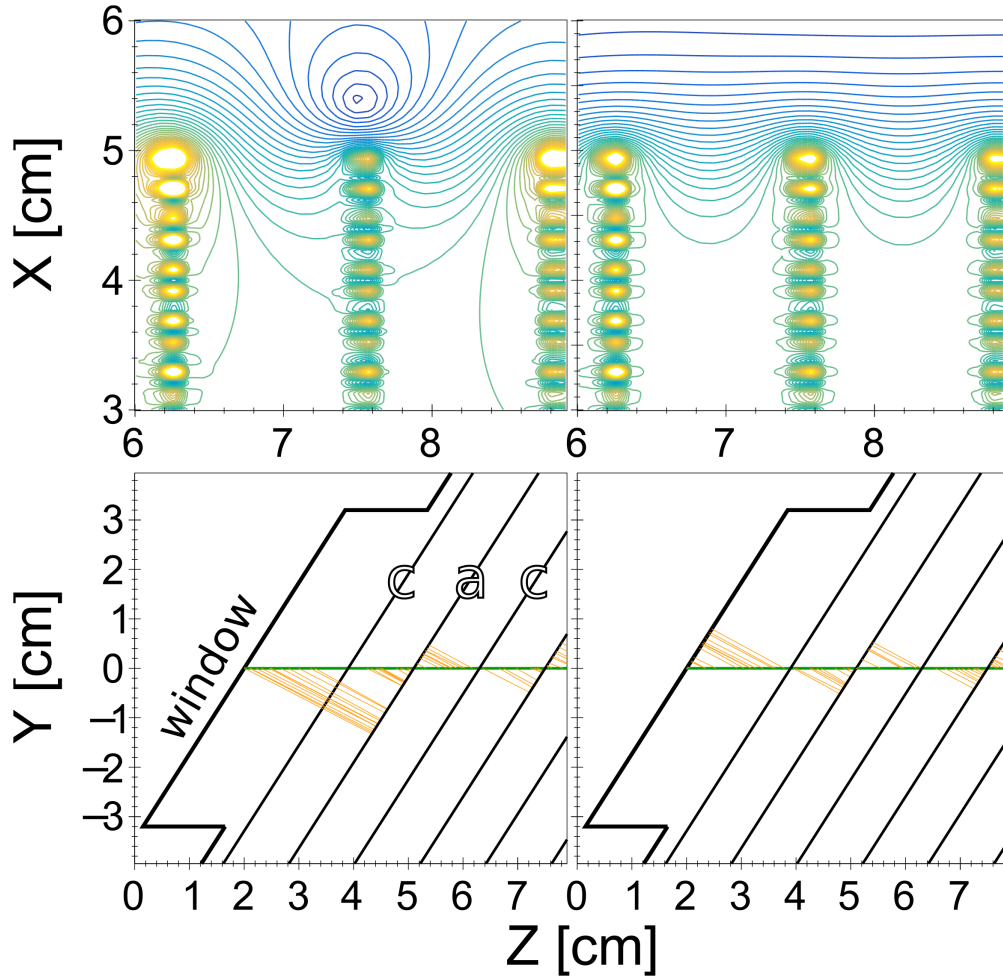
11

Figure 5: Field map contours (top) and electron drift lines (bottom) calculated by Garfield++ for a constant potential difference of 244 V between the cathode and anode grids. [Left] Cathode voltage = 0 V, anode voltage = +244 V. [Right] Cathode voltage = −122 V, anode voltage = +122 V. Electron drift lines (thin orange lines) from the beam ionization track (thick green lines) are shown in the bottom two panels. The Mylar entrance window, cathode (c) and anode (a) grids are labeled on the bottom left panel. (Color online).

use with TRIFIC [4]. The multiple-channel readout capability of the custom preamplifiers give TRIFIC a higher degree of segmentation than described in Ref. [1].

Three versions of the module have been constructed. In each, low-noise amplification is achieved using NXP BF862 JFETs [19] (J_1) with a noise specification of 0.8 nV/$\sqrt{\text{Hz}}$ at 100 kHz and ADI ADA4897-1 amplifiers [20] with a noise specification of 1 nV/$\sqrt{\text{Hz}}$ at 1 kHz. A preamplifier circuit is shown on Fig. 4 for a single TRIFIC channel. Different total gain and shaping times are set for each module. The first is a slow-decay ($R_F = 30$ MΩ, $C_F = 1.2$ pF, $\tau_{RC} = 36$ μs), high-gain (11×) module designed for off-line tests with α-particle sources, while the second and third modules have a fast-decay ($R_F = 1$ MΩ, $C_F = 1.2$ pF, $\tau_{RC} = 1.2$ μs) with low- (2×) and medium-gain (5×) respectively, for use in high-rate in-beam experiments at TIGRESS. The total power consumption of one 24 channel module is +6 V at 384 mA and -6 V at 144 mA. Each preamplifier module is housed in a shielded 60 × 110 × 30 mm ($l \times w \times h$) box. Individual TRIFIC electrodes are read out through a single channel as shown on Fig. 4 and input to a 100 MHz, 14 bit ADC on a GRIF-16 card in the GRIFFIN DAQ architecture [7]. Detector hit information such as time and charge are determined by the standard GRIFFIN digital signal processing algorithms described in Ref. [7], with optimization discussed in Sec. 3.2. Waveform traces can also be written to disk for further analysis.

TRIFIC was tested off-line using a Pu-Am-Cm 3α source. TRIFIC was operated with 91.2 Torr of CF_4 gas during these tests. The source

---

[4]A set of single-channel ORTEC 109a preamplifier modules were used with TRIFIC previously.

13

was mounted 5 mm from the first electrode and collimated through a 2 mm
aperture in order to collimate the emitted α particles along the z-axis of the
detector. A Bragg curve for the emitted particles was measured and is shown
in Fig. 6. The energy resolution of the individual grids is approximately 1.6
MeV which is not sufficient to resolve the three α-particle energies.

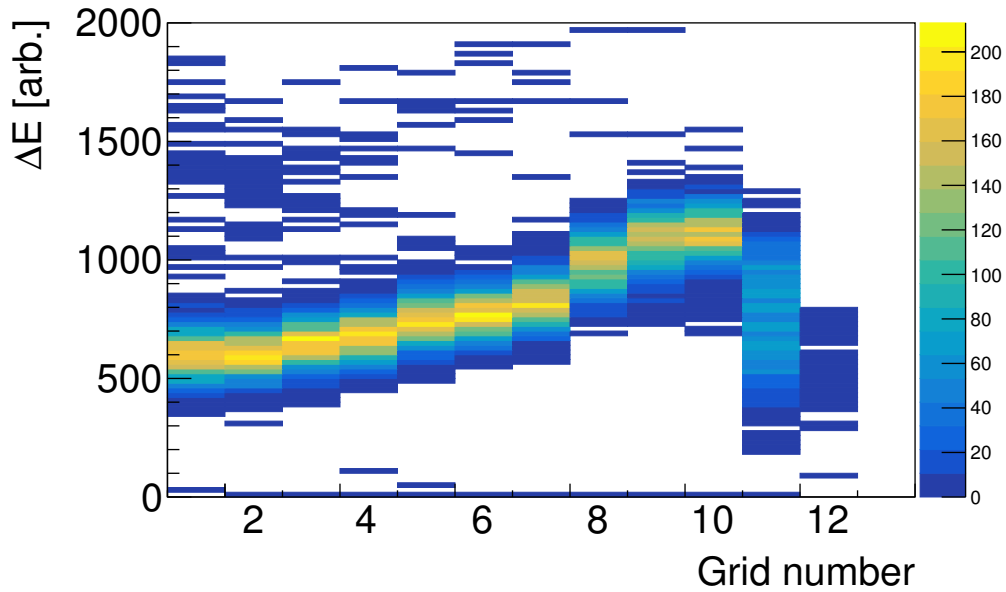Figure 6: Bragg curve showing the energy deposited in each grid versus the grid number measured for a 3α source. The approximately 1.6 MeV (FWHM/centroid) energy resolution is insufficient to resolve the three α emitters. (Color online).

2.3. Reduced field optimization

Off-line analysis of waveform traces from the individual grids was performed in order to minimize the charge collection time, which manifests as a shorter observed signal risetime. The charge collection time was minimized by minimizing the risetime as a function of the pressure-reduced field E/P by changing bias voltages applied to the anode and cathode grids while

14

keeping the CF_4 gas pressure constant at 91.2 Torr. A plot of the signal risetime against the reduced field is shown in Fig. 7. A third-order polynomial fit to the minimum gave an optimum pressure-reduced field E/P of approximately 2 V/cm/Torr. The behavior of the signal risetime at different reduced fields is governed by a complex interplay of many different factors which depend on the gas properties and charge collection process. A reduction in electron drift speed in CF_4 as the reduced field strength approaches 10 V/cm/Torr has been experimentally observed [21], and suggests that a monotonic dependence of the signal rise time as a function of the reduced field should not be expected. Instead, the detector performance was characterized and optimized. Due to differences in the preamplifier electronics, signal risetimes of $\approx$120 ns were observed in-beam using the fast-decay modules.

2.4. Gas handling system

Tetramethylflouride (CF_4) gas is the standard gas used with TRIFIC. Running the detector at a high count rate requires that the ion and electron transport in the gas is fast: CF_4 satisfies this requirement with respect to other perflouroalkanes [22], and has been used in other recently completed high-rate gas counters [1–4]. Additionally, the drift velocity does not saturate in the expected operating range ($E/P \approx$ 1–5 V/cm/Torr) of the detector [21]. Gas pressure inside TRIFIC is controlled during operation using a system consisting of an MKS Type 622C Baratron gauge for monitoring the gas pressure and an Omega CN76000 process controller operated by a MKS 247C mass flow controller power supply unit. Typical gas flow rates are on the order of 10 sccm, giving a total cycle time of approximately
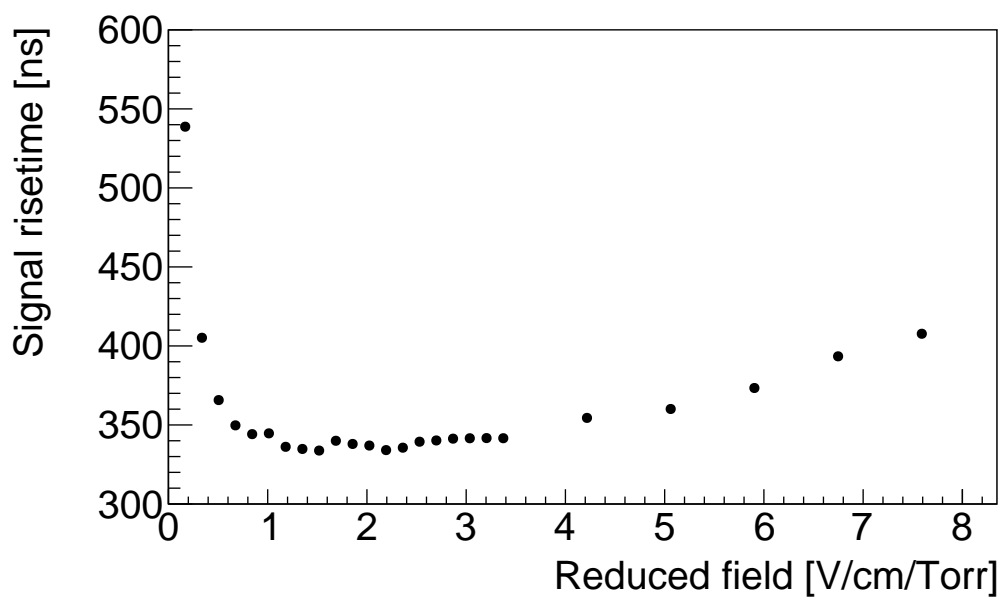
15

Figure 7: The observed signal risetime as a function of the reduced field. Risetime was defined as the time required for the signal to rise from 10% to 90% of it's maximum value. The CF$_4$ gas pressure was held constant at 91.2 Torr and the applied bias was varied. A minimum occurs at pressure-reduced field E/P of approximately 2 V/cm/Torr.

2 hours for 100 Torr operating pressure at 20° C.

3. TRIFIC commissioning

3.1. Resolving power

The Z resolving power of TRIFIC was tested experimentally in-beam with a cocktail beam consisting of ^{86}Kr ($Z = 36$) and ^{86}Sr ($Z = 38$) ions at an energy of 4 MeV/A (344 MeV). Contaminant species ^{63}Cu (252 MeV, $Z = 29$) and ^{40}Ar (160 MeV, $Z = 18$) were also identified in the beam provided by the TRIUMF Off-Line Ion Source (OLIS) [23]. During this test TRIFIC was operated with 60 Torr of CF_4 gas.

Incident charged particle species with different atomic number Z can be separated in TRIFIC due by the differences in their characteristic energy-loss Bragg curves. A particle identification (PID) plot of the energy loss in grids 1–5 (ΔE1) vs the energy deposited at the end of the ion's range in grids 15–19 (ΔE2) is shown in Fig. 8. Clear loci appear for the primary beam constituents ^{86}Kr and ^{86}Sr as well as the ^{63}Cu and ^{40}Ar contaminants originating from the ion source. Relative locations of the loci for the detected ions was determined using simulated energy loss curves. The vertically-distributed structures appearing below the ^{86}Kr peak on the ΔE2 axis result from the ion hitting one of the wires in the section of the detector where the ΔE2 signal is measured. These features are present for all species, but are most clearly visible for the most intense beam component ^{86}Kr. The data were taken at an incident beam rate of 1 kpps. A separation of 5.2σ between the centroids of ^{86}Kr and ^{86}Sr was determined from a bivariate normal distribution fit to the data. This leads to a resolving power

at 3 FWHM of $Z/\Delta Z \approx 14$ and a separability at 1 FWHM of $Z/\Delta Z \approx 42$ in the "beam monitor" mode.

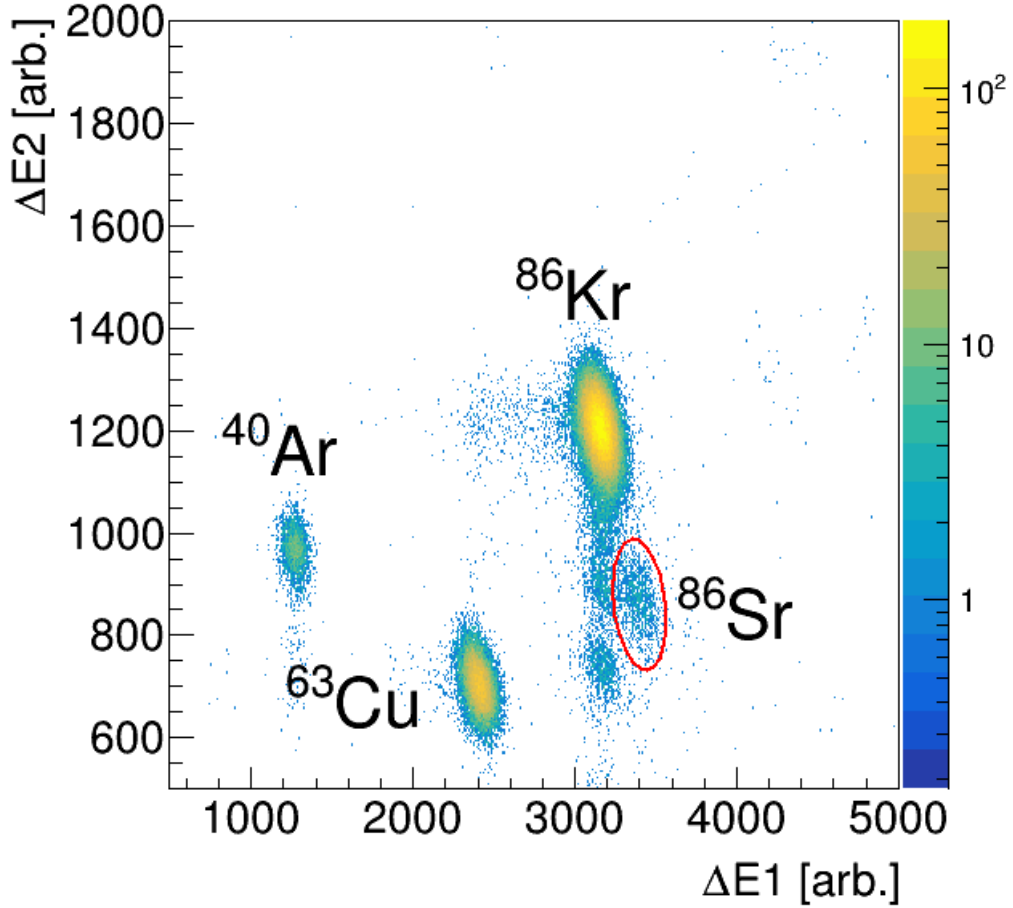Figure 8: A PID plot demonstrating the separation between various charged particle species ^{86}Sr ($Z = 38$) ^{86}Kr ($Z = 36$), ^{63}Cu ($Z = 29$) and ^{40}Ar ($Z = 18$) at a beam intensity of 1 kpps. A separation of 5.2σ between ^{86}Sr and ^{86}Kr was achieved by plotting energy loss recorded in grids 1–5 ($\Delta E1$) against the energy loss in grids 15–19 ($\Delta E2$). The structures distributed vertically below the ^{86}Kr peak result from the ion hitting one of the wires in the $\Delta E2$ section. (Color online).

3.2. High rate performance

The high-rate performance of TRIFIC was assessed at beam intensities of up to 500 kpps. For these tests, TRIFIC was operated at 95 Torr CF_4. A pure beam of ^{40}Ar at 6.75 MeV/A (270 MeV) was provided by OLIS.

Signal processing parameters of the GRIFFIN DAQ software described in Ref. [7] were optimized in order to operate TRIFIC with beam intensities up to 500 kpps. Parameters of the pulse-height evaluation algorithm were chosen such that the evaluation occurred in under 1 μs. Signal differentiation and integration shaping parameters were set to 260 ns and 200 ns, respectively. Pole-zero correction parameters were optimized on a channel-by-channel basis at low rate. The range of the pole zero parameters was 1.063–1.205 μs, in good agreement with the nominal preamplifier decay constant $\tau_{RC} = 1.2$ μs. Following these optimization steps, the beam intensity was increased in steps up to 500 kpps to assess the detector performance. The performance of the detector was analyzed at beam intensities of 10, 50, 150, and 500 kpps. In the presented data the DAQ was operated in a pileup-rejection mode for optimum resolution, with an enforced deadtime of 250 ns between accepted events. Operating in this mode, at 500 kpps 23% of events are lost. The DAQ can alternatively be used in pileup-processing mode [7], in which case only 12% of events cannot be resolved due to coincidence summing and pileup.

Energy distributions corresponding to the interaction of a single ^{40}Ar ion in the first anode grid were fit with a skewed Gaussian function in order to determine the energy resolution. The measured energy distributions in the first anode grid of TRIFIC are shown in Fig. 9 and the corresponding resolutions determined from the fit to the data are presented in Table 1.
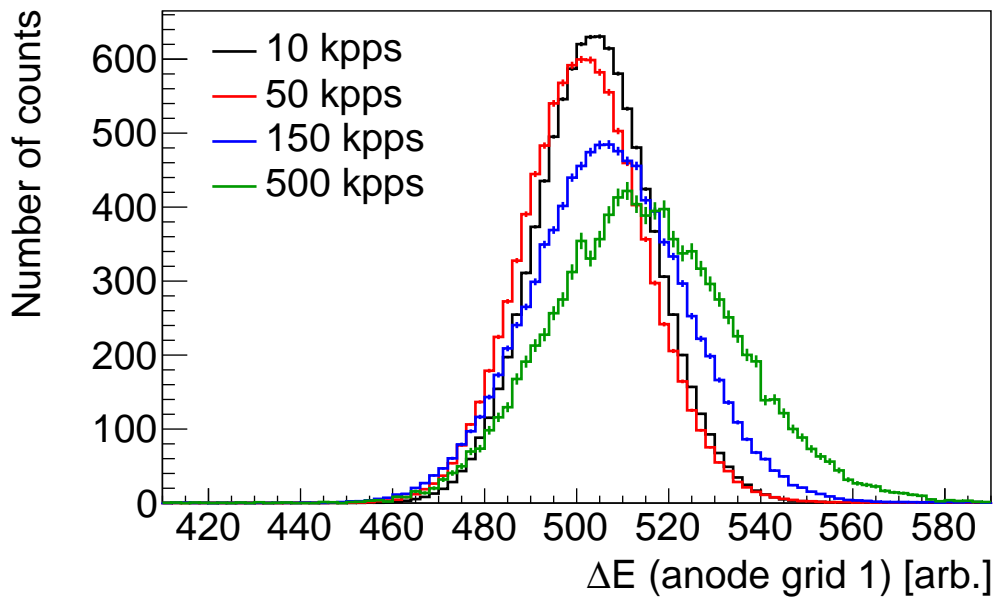
19

Figure 9: Energy distributions in the first anode grid of TRIFIC measured at 10, 50, 150, and 500 kpps demonstrating the change in energy resolution as a function of beam intensity. The distributions have been normalized to have the same area. The resolutions determined from fitting a skewed Gaussian to the data are given in Table 1. (Color online).

Up to 50 kpps, almost no change in the resolution was observed. Increasing the beam rate to 150 kpps resulted in energy resolution which was approximately 30% worse than the low-intensity data. At 500 kpps the resolution was approximately 50% worse. In all cases, the energy resolution given by FWHM/centroid was measured to be less than 10%. TRIM [16] calculations of the first anode signal region determined the energy straggling to be 1.8% of the mean energy deposited. The transmission per grid was measured to be ≈98.5% to each successive grid, consistent with the 99% transmission per grid expected from the design.

Table 1: Measured energy resolution (FWHM/centroid) of the first anode grid in TRIFIC as a function of the beam intensity determined by fitting the data shown in Fig. 9 with a skewed Gaussian function. The uncertainties at 1σ are given in parenthesis.

Beam intensity [kpps]	Resolution [%]
10	5.910(5)
50	6.234(9)
150	7.714(15)
500	9.01(5)

3.3. Operation of TRIFIC with TIGRESS

Operation of TRIFIC in coincidence with TIGRESS in the "recoil tagging" mode is an important feature of the detector as described in Sec. 1.1. A test experiment to identify the reaction products of the ^{40}Ar + d reaction on an event-by-event basis was performed. The TRIFIC setup and ^{40}Ar beam properties were the same as described in Sec. 3.2. Four TIGRESS detectors were placed at 90° relative to the beam axis and a 5 mg/cm^2 CD$_2$

21

³⁰⁵ (deuterated polyethylene) target was installed at the target position. Data
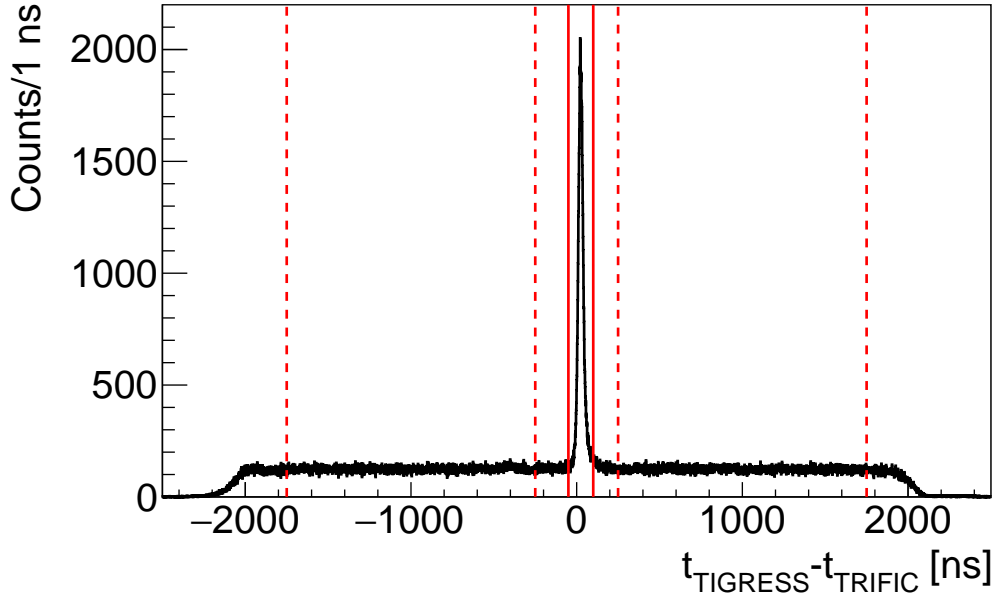³⁰⁶ were collected for approximately 15 hours with a beam intensity of 10 kpps.

Figure 10: Time coincidence spectrum between events in TIGRESS and the first anode grid of TRIFIC. The gating region for coincident events is shown by the solid lines and the gating region for time-random events used for suppression of background is shown by the dashed lines. (Color online).

³⁰⁷ Timing information for measured detector hits was determined using
³⁰⁸ the event timestamps and the CFD algorithm in the GRIFFIN DAQ. The
³⁰⁹ time difference between events in TIGRESS and events in the first anode
³¹⁰ grid of TRIFIC was used to identify the coincident detection of a γ-ray
³¹¹ in TIGRESS and a beam-like heavy ion in TRIFIC. The time difference
³¹² spectrum is shown in Fig. 10. A 150-ns wide time gate was set around the 32
³¹³ ns FWHM prompt-coincidence peak. Time-random events were identified
³¹⁴ for background subtraction in the analysis of the γ-ray data.
³¹⁵ In order to identify the reaction products of interest, a PID plot similar
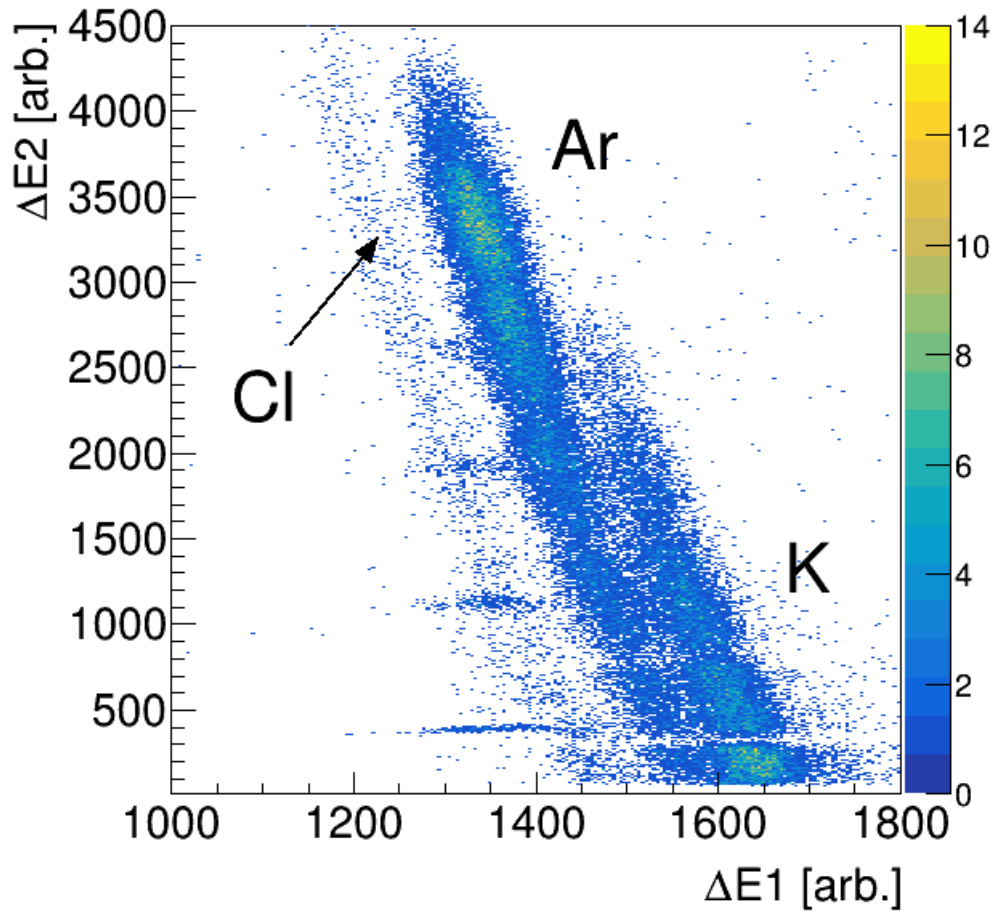
22

Figure 11: A particle identification plot for the TIGRESS test experiment described in Sec. 3.3. Beam-like Cl, Ar, and K nuclei are separated by plotting the summed energy deposits in grids 1 and 2 (ΔE1) against summed energy deposits in grids ≥ 6 (ΔE2). For a detailed discussion of the structure of this plot refer to Sec. 3.3. (Color online).
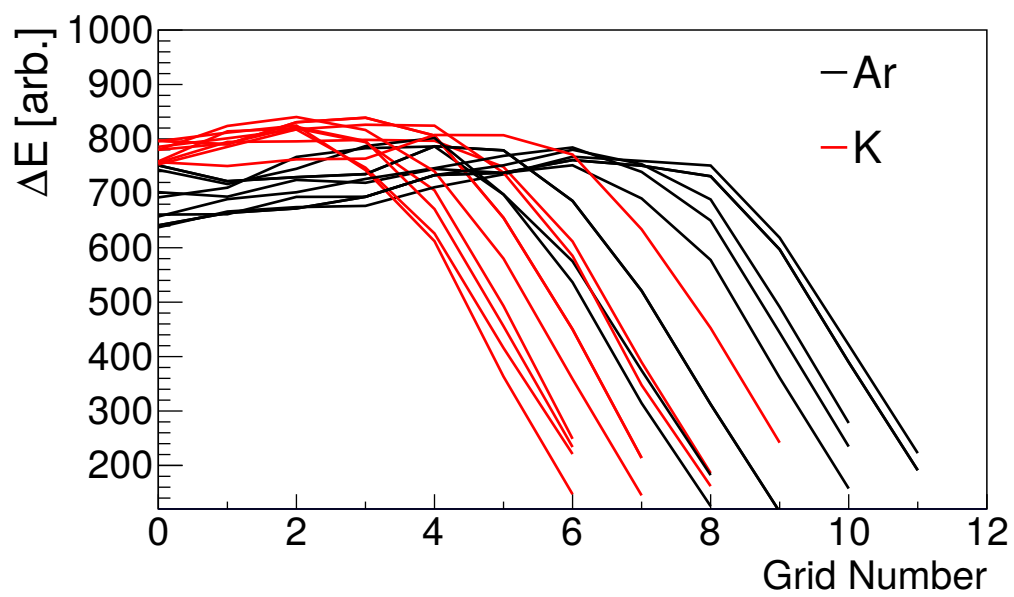
Figure 12: Particle-gated Bragg curve traces for Ar and K in coincidence with events in TIGRESS. Ten traces are shown for each ion. Each trace shows the grid-by-grid energy deposits for a single ion interacting in TRIFIC. The two nuclei with $\Delta Z = 1$ can be distinguished by a combination of the energy deposits and ion range. (Color online).

to that shown in Fig. 8 was constructed. Energy deposits in grids 1 and 2 were summed to define the ΔE1 signal and the ΔE2 signal was taken from the summed energy deposits in grids ≥ 6. The resultant PID plot of TRIFIC events in coincidence with TIGRESS demonstrating a clean identification of Ar, K, and Cl recoils is shown in Fig. 11. Substructures in Fig. 11 result from the combination of multiple grids. Vertical gaps, seen in the Ar and K loci, result from the energy thresholds of the individual grids present in the summing region chosen to define the ΔE2 signals. Vertically-distributed structures observed between ΔE1 = 1300 and ΔE1 = 1400 result from incident Ar ions hitting one of the wires in the ΔE2 summing region, similar to those appearing on Fig. 8 and discussed in Sec. 3.1.

Gates were set in the PID spectra on the three identified ion species. Bragg curves gated on the Ar and K distributions identified in Fig. 11 are shown in Fig. 12, demonstrating that the two nuclei with $\Delta Z = 1$ are clearly distinguished by their stopping powers. The broad range distributions shown in Fig. 11 arise from a combination of the reaction Q-values and the wide range of possible reaction energies due to the energy loss in the thick target. Particle-gated γ-ray spectra for events coincident with the detection of Ar, K, or Cl nuclei are shown in Figs. 13, 14, and 15 respectively. The γ-ray energies have been Doppler-corrected due to the decay in flight and a background subtraction of time-random events was performed.

A number of transitions in ^{41}Ar associated with the ^{40}Ar(d, p)^{41}Ar reaction were observed. The 167.1 keV $\frac{5}{2}_1^- \rightarrow \frac{7}{2}_{\text{g.s.}}^-$ transition, 348.7 keV $\frac{3}{2}_1^- \rightarrow \frac{5}{2}_1^-$ transition, 516.0 keV $\frac{3}{2}_1^- \rightarrow \frac{7}{2}_{\text{g.s.}}^-$ transition, and the 1186.6 keV $\frac{3}{2}_2^- \rightarrow \frac{5}{2}_1^-$ transition were identified in the data. Also present is the 1460.8 keV $2_1^+ \rightarrow 0_{\text{g.s.}}^+$ transition from inelastic excitation of the ^{40}Ar beam. Tran-

sitions in ^{40}K following the ^{40}Ar(d,2n)^{40}K reaction were also observed. Two γ-rays in this nucleus were identified: the first at 770.3 keV resulting from the $2_1^- \rightarrow 4_{\text{g.s.}}^-$ transition and the second at 891.4 keV from the $5_1^- \rightarrow 4_{\text{g.s.}}^-$ transition. No transitions from other isotopes were conclusively identified in the K gated spectrum. Previous studies [24] found that the ^{40}Ar(d,n)^{41}K channel primarily populates the ground state and $\frac{7}{2}_1^-$ state. Due to the long lifetime of the $\frac{7}{2}_1^-$ state, no γ-rays are expected to be observed. In the Cl gated spectrum, the 1745.7 keV $0^-, 1^- \rightarrow 2_{\text{g.s.}}^-$ transition in ^{38}Cl following the ^{40}Ar(d,α)^{38}Cl reaction was observed and is shown on Fig. 15.
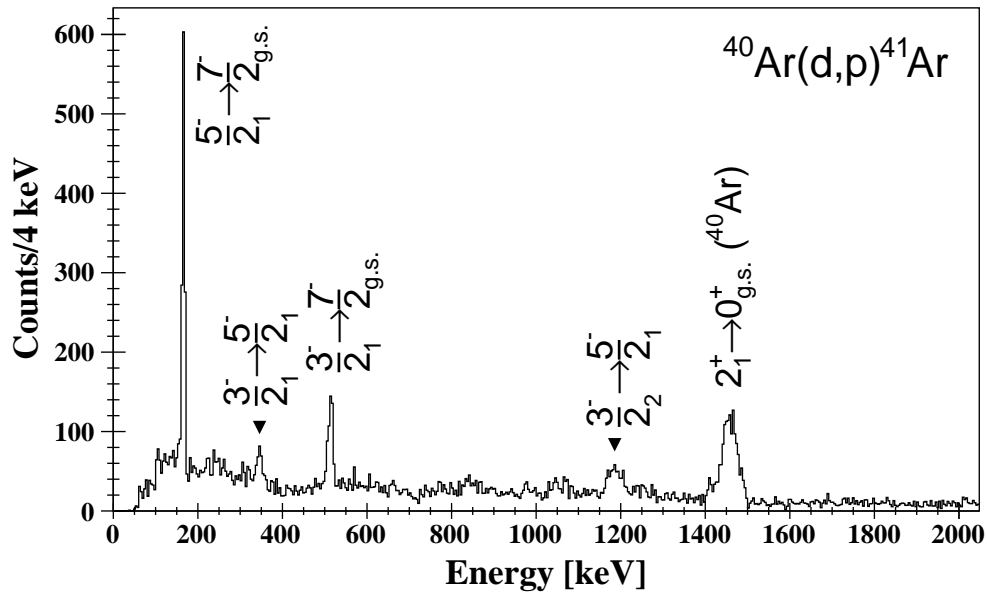

Figure 13: Doppler-corrected, background-subtracted γ-ray spectrum in coincidence with the detection of an Ar nucleus in TRIFIC. Known transitions in ^{41}Ar observed following the the ^{40}Ar(d, p)^{41}Ar reaction are labeled. The 1460.8 keV transition from the inelastic excitation of the ^{40}Ar beam is also shown.

Gamma-rays were successfully detected in coincidence with events in

26

TRIFIC at 10 kpps. The various reaction products of the ^{40}Ar + d reaction could be identified by their characteristic energy loss in the gas. Clean separation of γ-rays arising from decays in ^{40,41}Ar, ^{40}K and ^{38}Cl presented in Figs. 13–15 demonstrates the power of the "recoil tagging" of heavy ions on an event-by-event basis.
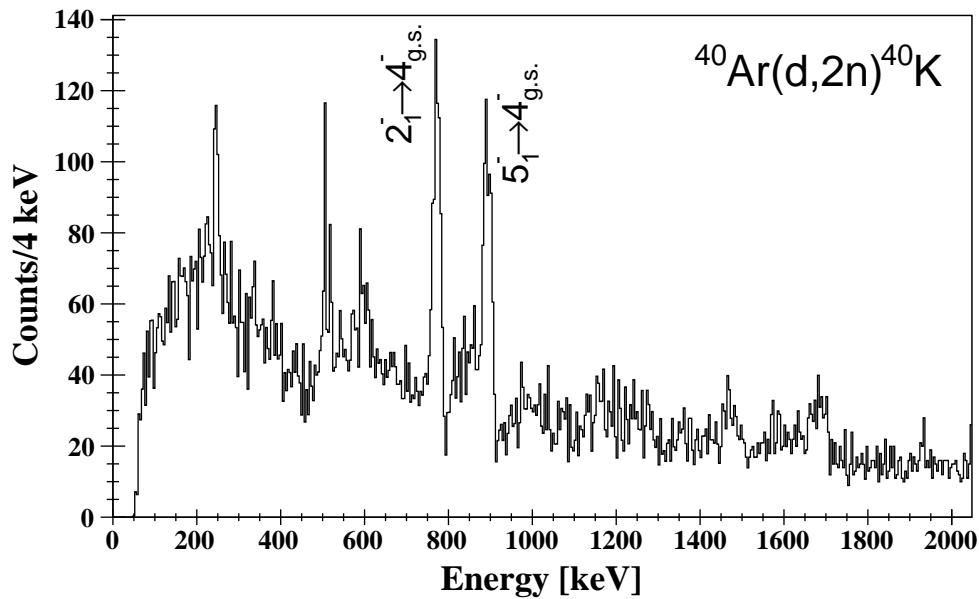

Figure 14: Doppler-corrected, background-subtracted γ-ray spectrum in coincidence with the detection of an K nucleus in TRIFIC. Known transitions in ^{40}K observed following the ^{40}Ar(d,2n)^{40}K reaction are labeled.

4. Conclusions

The TRIFIC gas ionization chamber was constructed and commissioned for RIB experiments at TRIUMF-ISAC. Custom-built fast electronics were developed to enable individual grid readout of electrode signals from TRIFIC at high rate. The TRIFIC detector was commissioned following two exper-
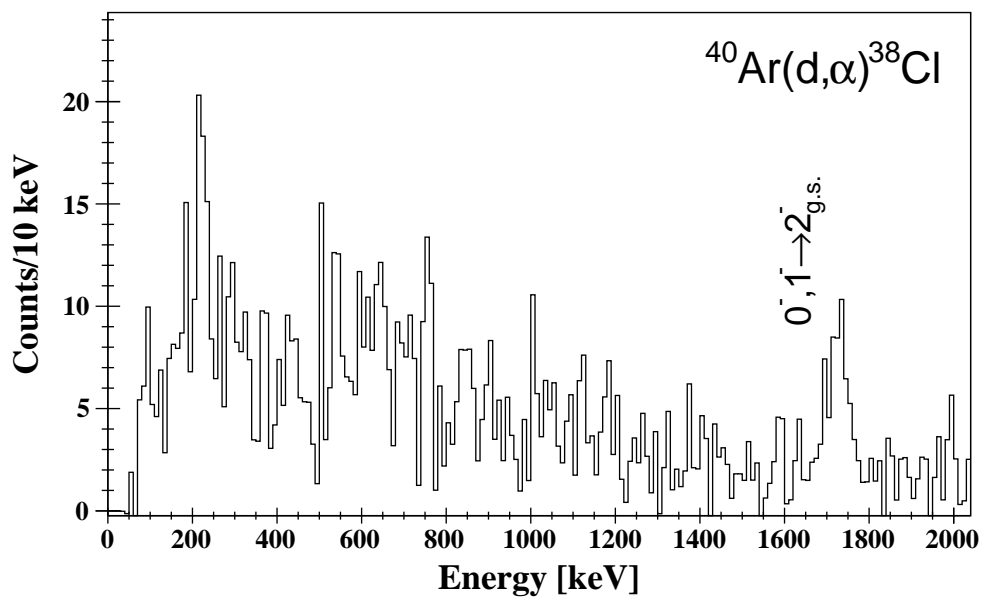
27

Figure 15: Doppler-corrected, background-subtracted γ-ray spectrum in coincidence with the detection of a Cl nucleus in TRIFIC. One known transition in ^{38}Cl observed following the the ^{40}Ar(d, α)^{38}Cl reaction is labeled.

iments using ^{86}Kr/^{86}Sr and ^{40}Ar beams at intensities up to 500 kpps with a GRIF-16-based digital DAQ system. A resolving power at 3 FWHM of $Z/\Delta Z \approx 14$ and a separability at 1 FWHM of $Z/\Delta Z \approx 42$ at $Z \approx 40$ has been demonstrated. Gamma-ray spectra recorded by TIGRESS in coincidence with TRIFIC demonstrated the viability of event-by-event identification of beam-like heavy ions. TRIFIC has been successfully commissioned in "beam monitor" mode for beam intensities up to 50 Mpps when using the two $\times 0.1$ attenuator foils. Alternative grid designs which enable scattering angle sensitivity have been designed and will be tested.

Acknowledgements

References

[1] K. Y. Chae, S. Ahn, D. W. Bardayan, K. A. Chipps, B. Manning, S. D. Pain, W. A. Peters, K. T. Schmitt, M. S. Smith, S. Y. Strauss, Construction of a fast ionization chamber for high-rate particle identification, Nuclear Instruments and Methods in Physics Research Section A: Accelerators, Spectrometers, Detectors and Associated Equipment 751 (2014) 6–10.

[2] J. Vadas, V. Singh, G. Visser, A. Alexander, S. Hudan, J. Huston, B. B. Wiggins, A. Chbihi, M. Famiano, M. M. Bischak, R. T. deSouza, High-rate axial-field ionization chamber for particle identification of radioactive beams, Nuclear Instruments and Methods in Physics Research Section A: Accelerators, Spectrometers, Detectors and Associated Equipment 837 (2016) 28–33.

[3] M. S. Kwag, K. Y. Chae, S. M. Cha, A. Kim, M. J. Kim, E. J. Lee, J. H. Lee, Construction and commissioning of a position-sensitive ionization chamber, Journal of the Korean Physical Society 68 (2016) 1165–1169.

[4] J. Lai, L. Afanasieva, J. C. Blackmon, C. M. Deibel, H. E. Gardiner, A. Lauer, L. E. Linhardt, K. T. Macon, B. C. Rasco, C. Williams, D. Santiago-Gonzalez, S. A. Kuvin, S. Almaraz-Calderon, L. T. Baby, J. Baker, J. Belarge, I. Wiedenhöver, E. Need, M. L. Avila, B. B. Back, B. DiGiovine, C. R. Hoffman, Position-sensitive, fast ionization chambers, Nuclear Instruments and Methods in Physics Research Section A: Accelerators, Spectrometers, Detectors and Associated Equipment 890 (2018) 119–125.

[5] G. Hackman, C. E. Svensson, The TRIUMF-ISAC gamma-ray escape suppressed specrometer, TIGRESS, Hyperfine Interactions 225 (2014) 241–251.

[6] R. E. Laxdal, Acceleration of radioactive ions, Nuclear Instruments and Methods in Physics Research Section B: Beam Interactions with Materials and Atoms 204 (2003) 400–409. 14th International Conference on Electromagnetic Isotope Separators and Techniques Related to their Applications.

[7] A. B. Garnsworthy, C. J. Pearson, D. Bishop, B. Shaw, J. K. Smith, M. Bowry, V. Bildstein, G. Hackman, P. E. Garrett, Y. Linn, J.-P. Martin, W. J. Mills, C. E. Svensson, The GRIFFIN data acquisition system, Nuclear Instruments and Methods in Physics Research Section A: Accelerators, Spectrometers, Detectors and Associated Equipment 853 (2017) 85–104.

[8] C. A. Diget, S. P. Fox, A. Smith, S. Williams, M. Porter-Peden, L. Achouri, P. Adsley, H. Al-Falou, R. A. E. Austin, G. C. Ball, J. C. Blackmon, S. Brown, W. N. Catford, A. A. Chen, J. Chen, R. M. Churchman, J. Dech, D. D. Valentino, M. Djongolov, B. R. Fulton, A. Garnsworthy, G. Hackman, U. Hager, R. Kshetri, L. Kurchaninov, A. M. Laird, J. P. Martin, M. Matos, J. N. Orce, N. A. Orr, C. J. Pearson,

C. Ruiz, F. Sarazin, S. Sjue, D. Smalley, C. E. Svensson, M. Taggart, E. Tardiff, G. L. Wilson, SHARC: Silicon Highly-segmented Array for Reactions and Coulex used in conjunction with the TIGRESS γ-ray spectrometer, Journal of Instrumentation 6 (2011) P02005.

[9] E. Kwan, C. Y. Wu, N. Summers, G. Hackman, T. E. Drake, C. Andreoiu, R. Ashley, G. C. Ball, P. C. Bender, A. J. Boston, H. C. Boston, A. Chester, A. Close, D. Cline, D. S. Cross, R. Dunlop, A. Finlay, A. B. Garnsworthy, A. B. Hayes, A. T. Laffoley, T. Nano, P. Navrátil, C. J. Pearson, J. Pore, S. Quaglioni, C. E. Svensson, K. Starosta, I. J. Thompson, P. Voss, S. J. Williams, Z. M. Wang, Precision measurement of the electromagnetic dipole strengths in ^{11}Be, Physics Letters B 732 (2014) 210–213.

[10] S. Cruz, P. C. Bender, R. Krücken, K. Wimmer, F. Ames, C. Andreoiu, R. A. E. Austin, C. S. Bancroft, R. Braid, T. Bruhn, W. N. Catford, A. Cheeseman, A. Chester, D. S. Cross, C. A. Diget, T. Drake, A. B. Garnsworthy, G. Hackman, R. Kanungo, A. Knapton, W. Korten, K. Kuhn, J. Lassen, R. Laxdal, M. Marchetto, A. Matta, D. Miller, M. Moukaddam, N. A. Orr, N. Sachmpazidi, A. Sanetullaev, C. E. Svensson, N. Terpstra, C. Unsworth, P. J. Voss, Shape coexistence and mixing of low-lying 0^+ states in ^{96}Sr, Physics Letters B 786 (2018) 94–99.

[11] G. L. Wilson, W. N. Catford, C. A. Diget, N. A. Orr, P. Adsley, H. Al-Falou, R. Ashley, R. A. E. Austin, G. C. Ball, J. C. Blackmon, A. J. Boston, H. J. Boston, S. M. Brown, A. A. Chen, J. Chen, R. M. Churchman, D. S. Cross, J. Dech, M. Djongolov, T. E. Drake, U. Hager, S. P. Fox, B. R. Fulton, N. Galinski, A. B. Garnsworthy, G. Hackman, D. Jamieson, R. Kanungo, K. Leach, J.-P. Martin, J. N. Orce, C. J. Pearson, M. Porter-Peden, F. Sarazin, S. Sjue, C. Sumithrarachchi, C. E. Svensson, S. Triambak, C. Unsworth, R. Wadsworth, S. J. Williams, the Tigress collaboration, Towards 26 na via (d,p) with sharc and tigress and a novel zero-degree detector, Journal of Physics: Conference Series 381 (2012) 012097.

[12] A. Görgen, Shapes and collectivity of exotic nuclei via low-energy Coulomb excitation, Journal of Physics G: Nuclear and Particle Physics 37 (2010) 103101.

[13] M. Zielińska, L. P. Gaffney, K. Wrzosek-Lipska, E. Clément, T. Grahn, N. Kesteloot, P. Napiorkowski, J. Pakarinen, P. Van Duppen, N. Warr, Analysis methods of safe

Coulomb-excitation experiments with radioactive ion beams using the GOSIA code, The European Physical Journal A 52 (2016) 99.

[14] P. Ruotsalainen, J. Henderson, G. Hackman, G. H. Sargsyan, K. D. Launey, A. Saxena, P. C. Srivastava, S. R. Stroberg, T. Grahn, J. Pakarinen, R. Julin, P. T. Greenlees, C. A. J. Smallcombe, G. C. Ball, N. Bernier, M. Bowry, M. Buckner, R. Caballero-Folch, A. Chester, S. Cruz, L. J. Evitts, R. Fredrick, A. B. Garnsworthy, M. Holl, A. Kurkjian, D. Kisliuk, K. G. Leach, E. McGee, J. Measures, D. Mücher, J. Park, F. Sarazin, J. K. Smith, D. Southall, K. Starosta, C. E. Svensson, K. Whitmore, M. Williams, C. Y. Wu, Isospin symmetry in the lower sd shell: Coulomb excitation study of ^{21}Mg, arXiv preprint arXiv:1811.00774 (2018).

[15] J. Henderson, G. Hackman, P. Ruotsalainen, S. R. Stroberg, K. D. Launey, J. D. Holt, F. A. Ali, N. Bernier, M. A. Bentley, M. Bowry, R. Caballero-Folch, L. J. Evitts, R. Frederick, A. B. Garnsworthy, P. E. Garrett, B. Jigmeddorj, A. I. Kilic, J. Lassen, J. Measures, D. Muecher, B. Olaizola, E. O'Sullivan, O. Paetkau, J. Park, J. Smallcombe, C. E. Svensson, R. Wadsworth, C. Y. Wu, Testing microscopically derived descriptions of nuclear collectivity: Coulomb excitation of ^{22}Mg, Physics Letters B 782 (2018) 468–473.

[16] J. F. Ziegler, M. D. Ziegler, J. P. Biersack, SRIM–The stopping and range of ions in matter (2010), Nuclear Instruments and Methods in Physics Research Section B: Beam Interactions with Materials and Atoms 268 (2010) 1818–1823.

[17] Data Sheet, MHV-4 4 channel, 800 V detector bias supply, mesytec GmbH & Co. KG, Wernher-von-Braun-Str. 1, 85640 Putzbrunn, Germany, 4.0_02 edition, 2018. Retrieved from: https://www.mesytec.com/products/datasheets/MHV-4.pdf. Accessed 11 January 2019.

[18] H. Schindler, Garfield++ User Guide, 2017. Retrieved from: https://garfieldpp.web.cern.ch/garfieldpp /documentation/UserGuide.pdf. Accessed 10 December 2018.

[19] Data Sheet, BF862 N-channel junction FET, NXP Semiconductors, High Tech Campus 60, 5656 AG Eindhoven, The Netherlands, 2000. Retrieved from: https://www.nxp.com/docs/en/data-sheet/BF862.pdf. Accessed 8 January 2019.

[20] Data Sheet, ADA4896-2/ADA4897-1/ADA4897-2, Analog Devices, Inc., One Tech-

480   nology Way, P.O. Box 9106, Norwood, MA 02062-9106, U.S.A., B edition, 2012. Re-

481   trieved from: https://www.analog.com/media/en/technical-documentation/data-

482   sheets/ADA4896-2_4897-1_4897-2.PDF. Accessed 8 January 2019.

483 [21] V. A. Lisovskiy, V. D. Yegorenkov, Electron-drift velocity determination in CF_4 and

484   SF_6 in a strong electric field from breakdown curves of low-pressure RF discharge,

485   Journal of Physics D: Applied Physics 32 (1999) 2645.

486 [22] S. R. Hunter, J. G. Carter, L. G. Christophorou, Electron motion in the gases CF_4,

487   C_2F_6, C_3F_8, and n-C_4F_{10}, Physical Review A 38 (1988) 58–69.

488 [23] K. Jayamanna, F. Ames, G. Cojocaru, R. Baartman, P. Bricault, R. Dube, R. Lax-

489   dal, M. Marchetto, M. MacDonald, P. Schmor, G. Wight, D. Yuan, Off-line ion

490   source terminal for isac at triumf, Review of Scientific Instruments 79 (2008) 02C711.

491 [24] M. Hagen, U. Janetzki, K.-H. Maier, H. Fuchs, The (d, n) reactions on even argon

492   isotopes, Nuclear Physics A 152 (1970) 404–418.